ARTICLE

An Interference Localized Surface Plasmon Resonance Biosensor Based on the Photonic Structure of Au Nanoparticles and SiO_2/Si Multilayers

Ha Minh Hiep,[†,‡] Hiroyuki Yoshikawa,[‡] Masato Saito,[‡] and Eiichi Tamiya[‡,*]

[†]School of Materials Science, Japan Advanced Institute of Science and Technology, 1-1, Asahidai, Nomi, Ishikawa 923-1292, Japan, and [‡]Department of Applied Physics, Graduate School of Engineering, Osaka University, 2-1 Yamadaoka, Suita, Osaka 565-0871, Japan

ABSTRACT This paper presents the experimental and simulation analysis of an original nanostructure design constructed with plasmonic gold nanoparticles and photonic thin-film multilayers of silicon dioxide (500 nm in thickness) and silicon on a substrate. Our nanostructure substrate showed a high sensitivity for various refractive index RI solutions and a prominent capacity for functionalizing alkanethiol molecules on the gold surface and demonstrates great potential in the development of a microfluidic-based biosensor for monitoring biotin−avidin interactions in real-time.

KEYWORDS: interference localized surface plasmon resonance (iLSPR) · photonic nanostructure · biosensors · biotin−avidin interaction · coupling plasmon · interference

*Address correspondence to tamiya@ap.eng.osaka-u.ac.jp.

Received for review November 16, 2008 and accepted January 22, 2009.

Published online February 4, 2009.
10.1021/nn800831a CCC: $40.75

The localized surface plasmon resonance (LSPR) of noble metal nanoparticles have been described in numerous articles.[1−9] Changes in the peak intensity and wavelength of plasmon spectra, which are caused by the refractive index (RI) variations that result from the binding of molecules to the metal nanoparticles are optically detectable parameters in biophotonics and biosensor devices.[10−13] However, the sensitivity and accuracy of current LSPR biosensors require further improvement for the field of analytical chemistry, owing to the unwanted noise that rises from the variants of nonspecific binding molecules.[14−16] In addition, finding a novel nanostructure design with special optical properties is always an attractive lure for researchers.

In this work, we report a vanguard combination of plasmonic metal nanoparticles and photonic thin-film multilayers on an interference LSPR (iLSPR) substrate. The thin-film multilayers of a silicon dioxide/silicon (SiO_2/Si) substrate consisting of transparent and semitransparent multilayers showed well-resolved Fabry−Perot fringes under light illumination. Such structures have been used for biosensors,[17,18] since the Fabry−Perot fringe pattern undergoes wavelength shifts upon molecule bindings. Additionally, it was established that a two-dimensional assembly of gold nanoparticles, which could be regarded as a thin film, still retained the optical characteristics of the original nanoparticles.[19,20] Inspired by the combination of these ideas, we took a pioneering step to propose an innovative multilayer nanostructure with the surface composed of gold nanoparticles. Experimental reflection spectra of our iLSPR substrate were numerically confirmed by simulations using a combination of complex Fresnel coefficients[21,22] and the Maxwell−Garnett effective medium theory.[23,24] When the RI of the surrounding medium increased, an obvious spectral band coupled with LSPR appeared in the interference pattern of the reflection spectrum. This indicates a great potential to develop novel iLSPR based biosensors for the label-free detection of biomolecules in an arbitrary solution.

RESULTS AND DISCUSSION

Our experimental setup for measuring the reflectance spectra of our substrates is illustrated in Figure 1a. The multilayered scheme of the iLSPR substrate is given in Figure 1b and an image of the surface, obtained with a scanning electron microscope (SEM), shown in Figure 1c. The gold nanoparticles monolayer was set to 50 nm thick on the SiO_2/Si substrate. The volume fraction of gold nanoparticles in this layer was 21.4 ± 0.9%.

Figure 2 panels a and b present reflection spectra of a bare SiO_2/Si substrate and

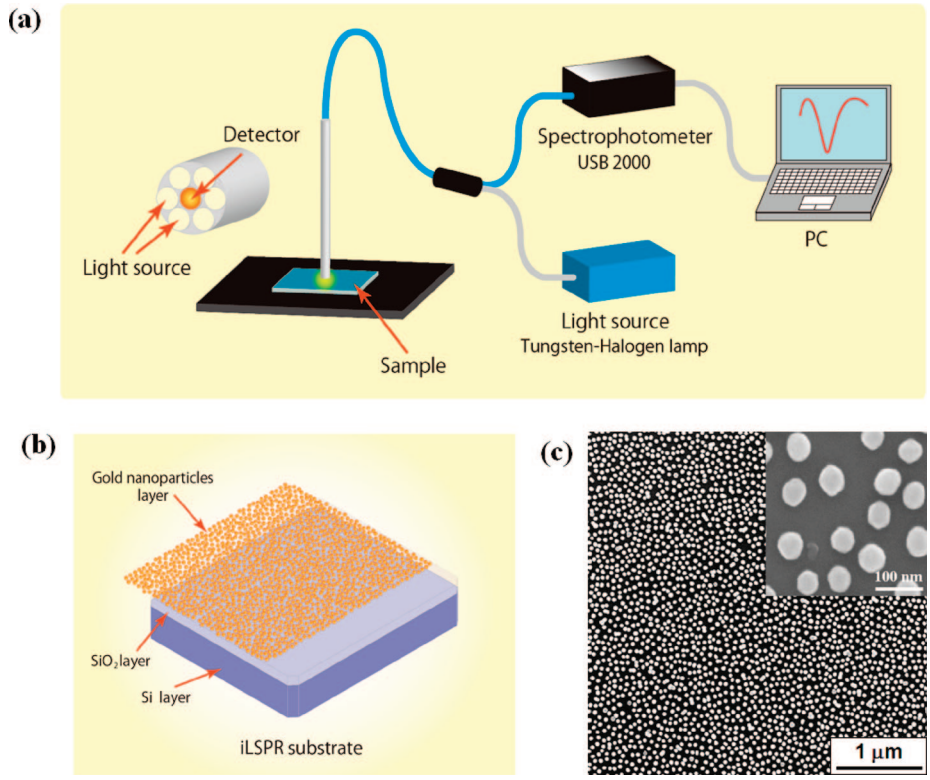

Figure 1. Optical system for measuring the reflectance spectra of our substrates: (a) experimental setup; (b) scheme of multilayers; (c) SEM images of iLSPR substrate.

the iLSPR substrate that were measured in air and oil. Both of the reflection spectra in Figure 2a show a similar fringe pattern. However, there was a noticeable difference between the two, when the substrates were immersed in oil as seen in Figure 2b. The low-contrast fringe pattern of the bare SiO_2/Si substrate was derived from the relative closeness of the RIs of the SiO_2 layer (RI = 1.46) and oil (RI = 1.516). On the other hand, the iLSPR substrate displayed an additional dark band (local minimum) around 540 nm with a high contrast fringe pattern. This band position corresponded to the plasmon band that appeared in the absorption spectrum, when a glass slide was covered to a similar degree with immobilized gold nanoparticles (see Supporting Information).

In the bare SiO_2/Si substrate, a relatively simple fringe pattern appeared in the reflection spectra. This fringe pattern was attributed to the interference of two light waves reflected by the substrate surface and the SiO_2/Si interface. On the other hand, phase matching condition between two light waves reflected by the substrate surface and the SiO_2/Si interface was strongly modulated by the gold-nanoparticle film in the iLSPR substrate, because the refractive index of gold nanoparticle layer drastically changed around 500−700 nm. Therefore, we could see constructive and destructive interferences attributed to phase changes induced by LSPR in the 500 to 700 nm region of reflection spectra. It means that both of two minima are influenced by LSPR. The minimum at about 540 nm is affected by LSPR more than that at about 680 nm, because it located closer to the LSPR peak wavelength.

We performed several actual calculations to augment our experimentally obtained reflection spectra. In this calculation model, a layer of immobilized gold nanoparticles was approximated by a dielectric thin film of 50 nm containing dispersed small particles. We attained the RI of this thin film using the Maxwell−Garnett effective medium theory. Figure 2c,d shows the simulated reflection spectra of the bare SiO_2/Si substrate and the iLSPR substrate under the same experimental conditions. In general, the reflection spectra obtained from both experiments and simulations were very similar. Nevertheless, in the simulation the computed dark band of the iLSPR substrate appeared at a shorter wavelength and its relative reflectance at ~500 nm was lower than that of the experiments (~600 nm). These discrepancies can probably be attributed to the Maxwell−Garnett approximation, when only the dipole (Fröhlich) mode of plasmon resonances was taken into account. It is obvious that the Maxwell−Garnett model that we used, not only has advantages in term of time reduction and simplicity compared to other approximation methods,[25,26] but also is a reliable and effective way to examine the

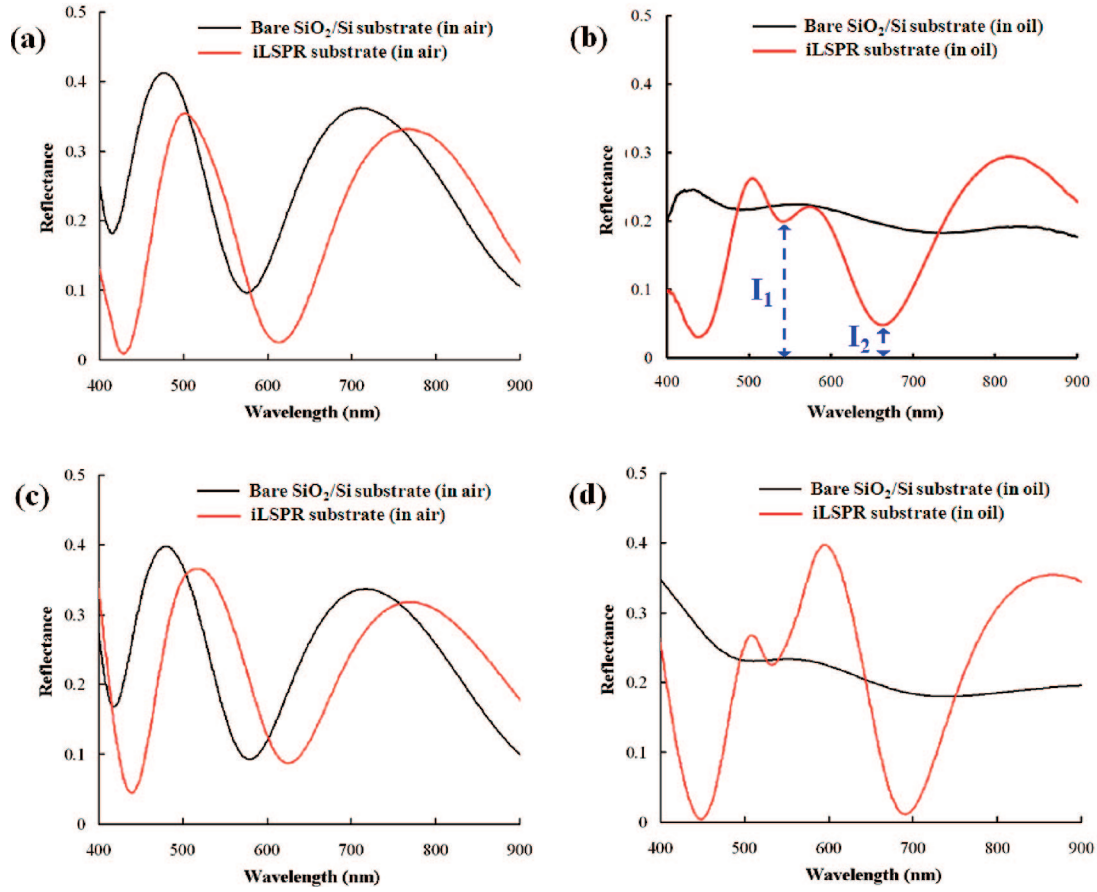

Figure 2. The experimental reflection spectra of bare SiO_2/Si substrate and iLSPR substrate were measured in air (RI = 1) (a) and oil (RI = 1.516) (b); numerical investigation of reflection spectra of bare SiO_2/Si substrate and iLSPR substrate measured in air (c) and measured in oil (d). The bulk optical constants of gold, Si, and SiO_2 were used in calculations of the Fresnel coefficients. The RI of the surrounding medium was the same as that of the dielectric film containing dispersed small gold nanoparticles on the SiO_2/Si substrate.

qualitative optical properties of our proposed nanostructure design.

The dependence of the iLSPR substrate's reflection spectra on SiO_2 layer thickness in both air and oil conditions was investigated and displayed as 2D color maps, as seen in the Figures 3a and 3b. In air, the number of dark (bright) bands increased with SiO_2 thickness and the band positions were shifted toward longer wavelengths, thus resulting in the 2D color map with diagonal stripes in Figure 3a. The distortions of the stripes around 500 nm were accredited to the LSPR band. In the high RI oil solution, the 2D color map showed a remarkable alteration: the diagonal stripes, made by dark bands, were interrupted at ~520 nm. This also indicated that the incident light, which went through and was reflected by the immobilized gold nanoparticle layer, experienced large phase changes at LSPR wavelengths.

The relation between the reflection spectra of iLSPR substrates and various solutions having different RIs was simulated and illustrated as a 2D color map in Figure 3c. Numerical results showed that in solutions with higher RI values a spectral band separated into two at LSPR wavelengths. However, the peak separation did not appear in a similar thin-film multilayers model constructed with a flat gold layer, 5 nm thick, deposited on a SiO_2/Si substrate, shown in Figure 3d. This confirmed the contribution of the plasmon band of gold nanoparticles in our iLSPR substrate. According to Fresnel's laws, in both cases a gradual change in the reflectance was a normal result of the increased bulk RI occurring on the gold surface. From the theoretical calculation results shown in Figure 3c, we defined the relative reflectance (RR) as follows:

$$RR = I_1/I_2, \quad (1)$$

where I_1 and I_2 are, respectively, the reflectance values at the left and right sides of the LSPR band from 550 to 650 nm, seen in Figure 1e. This enabled us to identify the local RI changes induced by the LSPR of our substrate. In our optical measurement, the shift of the broad LSPR band was converted to a large reflectance change by coupling to the interfer-

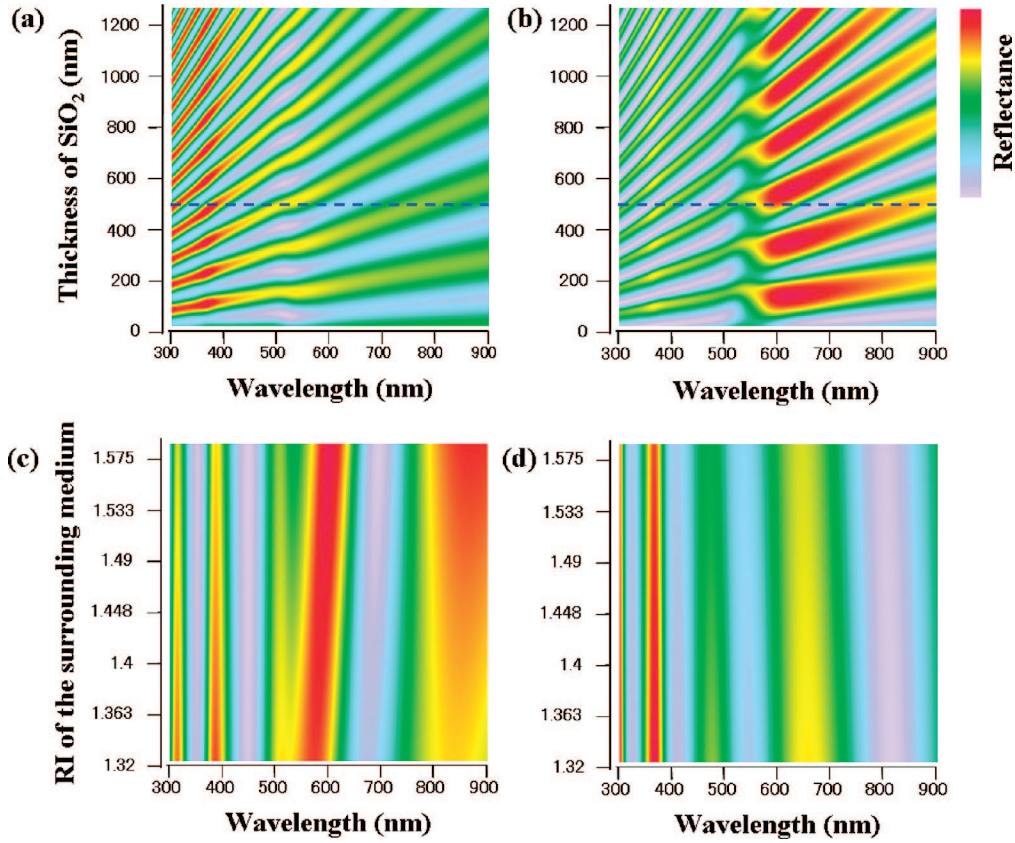

Figure 3. Dependency of reflection spectra of iLSPR substrate (containing gold nanoparticles of 50 nm) on SiO_2 layer thickness (a) in air, (b) in oil, and (c) on various RIs of surrounding media (the cross sections, recognized by blue broken lines in Figure 3a and 3b, corresponded to the reflection spectra in Figure 2a and 2b). In panel d the same computational method used for panel c was used in a similar thin-film multilayers model, constructed by a 5 nm thick flat gold layer deposited on a SiO_2/Si substrate.

ence. This relieved the laborious work of spectrum curve fitting which was necessary to determine the peak wavelength of the broad LSPR band.

As a corollary, the change in the LSPR band before and after chemical treatments of our interference substrates was evaluated by

$$\Delta RR = RR_{\text{after treatment}} - RR_{\text{before treatment}} \qquad (2)$$

The ability of our iLSPR substrate to convert the RI changes into a reflectance change is experimentally shown in Figure 4a using various solutions with different RIs. The results show that ΔRR also increases with the rise in the RIs of surrounding media. In the subsequent experiment, we investigated the surface-functionalized capacity of our substrate by incubating the gold surfaces with three alkanethiol molecules of 1 mM and different lengths ($CH_3(CH_3)_3SH$, $CH_3(CH_3)_5SH$ and $CH_3(CH_3)_9SH$) (Sigma-Aldrich Inc.) for 12 h. The longer carbon chain of alkanethiols resulted in a greater increase in the ΔRR, as illustrated in Figure 4b. This was consistent with previous observations,[27] in which the LSPR wavelength of triangular nanoparticles was shifted by few nm for each carbon atom in an absorbed alkanethiol molecule.

These achievements encouraged us to integrate our iLSPR substrate into a microfluidic-based biosensor for label-free, real-time monitoring of a specific biological model of biotin−avidin interactions (Figure 5a). To illustrate the bimolecular affinities, ΔRR was plotted as a function of time, as shown in Figure 5b. The microfluidic chip initially got an 11-amino-1-undecanethiol hydrochloride (Dojindo Laboratories, Japan) flow of 1 mM at the flow-rate of 5 μL/min until ΔRR reached a stable state. That process resulted in the formation of amino groups, which were able to react with solution of sulfosuccinimidyl 1-D-Biotin (Dojindo Laboratories) of 50 μg/mL *via* an ester link, on the gold surface. At the end of this step, a phosphate buffer saline (PBS) solution containing 10 μg/mL bovine serum albumin (BSA, Sigma-Aldrich Inc.) was applied to suppress nonspecific adsorption. An insignificant increment of ΔRR (ΔRR = 0.006) showed that there was only a slight absorption of BSA to the unreacted 11-amino-1-undecanethiol hydrochloride molecules or to the bare gold nanoparticles surface. The chip was then

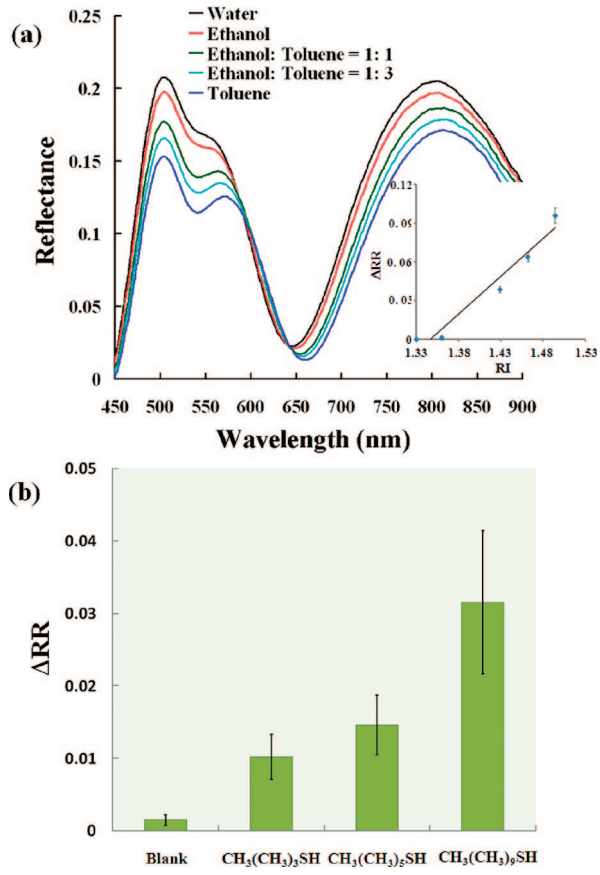

Figure 4. (a) Experimental evaluation of changes in the LSPR band of iLSPR substrates, when they were surrounded by water (RI = 1.33), ethanol (RI = 1.36), ethanol:toluene (1:1) (RI = 1.429), ethanol:toluene (1:3) (RI = 1.462), and toluene (RI = 1.459). The inset shows the dependence of ΔRR on refractive index values. (b) Alkanethiol chain length in relation to ΔRR of the plasmon band for iLSPR substrates (the blank sample did not contain any alkanethiol molecules).

filled with a flow of avidin solution (Sigma-Aldrich Inc.) of 10 μg/mL and the ΔRR approached an asymptotical equilibrium value after 15 min. The ability of BSA to effectively block nonspecific adsorption has been proven in earlier studies.[28−31] Thus, this result indicated that the increase of ΔRR was mainly caused by the specific biotin−avidin interactions.

We observed the ΔRR increments when various avidin concentrations were independently introduced into the biotinylated surface of microfluidic chips. Each concentration was repeated three times. Slight ΔRR increments in the buffer solution (without avidin) were caused by physical bindings but not by specific avidin−biotin interactions. With higher concentrations of avidin, ΔRR, denoting the interactions of avidin with biotinylated surface, increased constantly. That means the amount of bound avidin was directly related to the avidin concentrations. The mean increases in ΔRR for binding of various avidin concentrations of 0, 1, 10, and 100 μg/mL were 0.0025, 0.008, 0.031, and 0.044, respectively, as shown in Figure 6.

In conclusion, we have developed a novel plasmonic biosensor based on the combination of plasmonic gold nanoparticles and photonic thin-film multilayers. The unique plasmon property of our iLSPR substrate was manifested by the optical sensitivity of the binding of biomolecules to gold nanoparticles, and it was theoretically verified by calculation of the complex Fresnel coefficients combined with the Maxwell−Garnett effective medium theory.

In the previous LSPR sensors, the signal was represented as broadband and its intensity was weak because the interaction of incident light and gold nanoparticle only occurred once.[27,32] In our sensors, the shift of the broad LSPR band is converted to a large reflectance change and the multiple interactions of incident

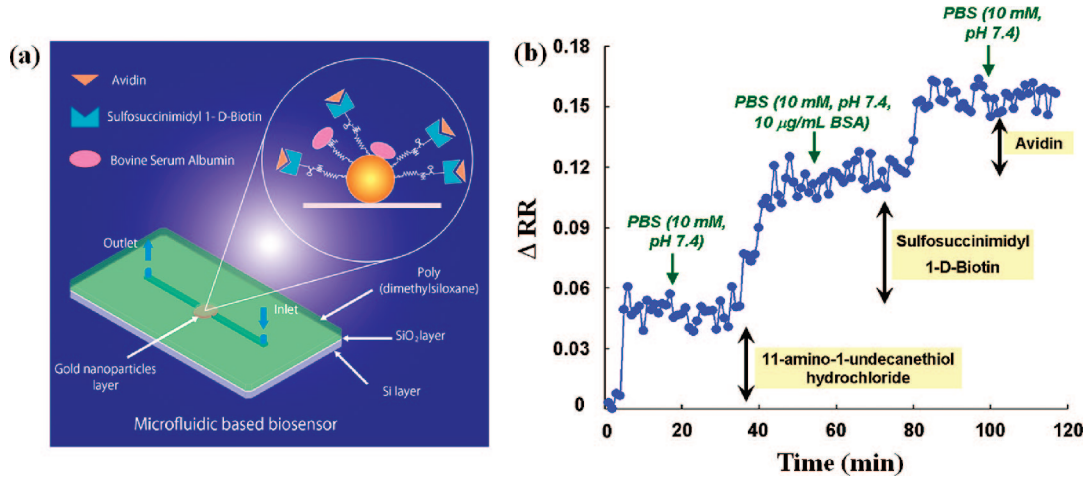

Figure 5. The microfluidic-based biosensors: (a) Diagram of the biosensor with its functionalized surface; (b) the sensorgram of 11-amino-1-undecanethiol hydrochloride, sulfosuccinimidyl 1-D-Biotin, and avidin molecules binding to the gold surface. PBS (20 mM, pH 7.4) was used to wash away the unbound molecules from the gold surface.

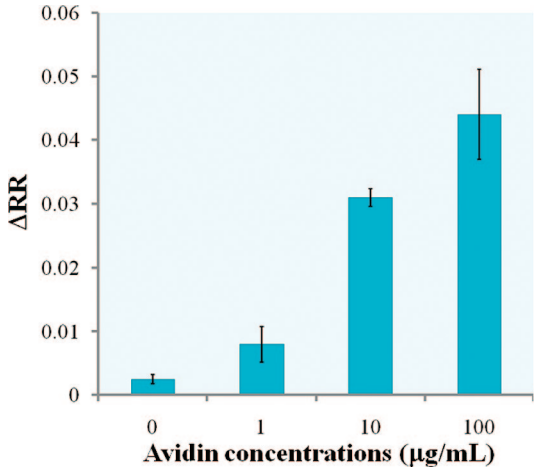

Figure 6. The dependence of ΔRR on various avidin concentrations.

light and gold nanoparticles can exist because the combination of the Si substrate and the gold-nanoparticle layer makes up a Fabry−Perot resonator. Theoretically, the reflectance change value can be considerably enhanced when a suitable matching condition between LSPR and interference spectra are established. To achieve the maximum sensitivity, further optimization steps of our structure on the aspects of density of immobilized gold-nanoparticles and thickness of SiO_2 are necessary. Although optimization works are more to be done, our nanostructure and analysis methods proposed in this work are promising. Future work will involve the dynamic range characterization, kinetic constant calculations, and steady-state-response estimations of our biosensor for other biomolecules, such as antigen−antibody interactions, and DNA hybridizations.

METHODS

Fabrication Process of iLSPR Substrate. The iLSPR substrates were fabricated by immobilizing gold nanoparticles, 50 nm in diameter, on a SiO_2/Si substrate. First, the SiO_2/Si substrate (Sumo Corporation, Japan) was cut into 1 × 1 cm^2 pieces, which were then soaked in a neutral pH detergent solution (Scat 20X-N, Dai-Ichi Kogyo Seiyaku, Japan) for 12 h. We cleaned the substrates in a 1:1:3 solutions of hydrogen peroxide (30%), ammonia (28%), and milliQ water for 30 min at 80 °C and completely washed them with milliQ water. Later, we immersed these substrates into 10% (v/v) solution of 3-aminopropyltrimethoxysilane for 15 min, rinsing with ethanol and drying at 120 °C for 2 h. Gold nanoparticles (British Biocell, UK) were dispersed as a monolayer on the modified SiO_2/Si substrates by absorbing for 24 h, and the monolayer was heated under vacuum conditions for 2 h. The bonding of gold nanoparticles to the surface was strong enough to resist detachment from the surface because of later chemical modifications. The surface of the immobilized gold nanoparticles layer on the SiO_2/Si substrate was imaged using a scanning electron microscope (SEM) (FEI Company, DB 235).

We used a standard soft-lithography technique to fabricate a microfluidic chip (500 μm thick) to cover the iLSPR substrate, using PDMS (Dow Corning, Japan). This chip contained a microchannel and a chamber. The created microchannel was 200 μm wide, 300 μm high, and 20 mm long. The chamber had the same diameter, 2 mm, as the surface area covered by the iLSPR substrate and a height of 300 μm. The inlet and outlet of the microfluidic device were connected to a fluorinated ethylene propylene (FEP) tube (0.15 ± 0.05 mm i.d.) and sealed with very small amounts of PDMS to prevent liquid leaks.

Optical Measurement System. We set up the following system to measure the reflection spectra: a spectrophotometer (USB-2000-UV−vis), a tungsten halogen light source (LS-1), and an optical fiber probe (R-400-7 UV/vis, fiber core diameter: 200 μm), all purchased from Ocean Optics. The sample substrate was placed proximately to the optical fiber probe surface so that the incident light was reflected upon hitting the sample surface and backed into the fiber probe. The sample was finally analyzed by UV−vis spectrophotometer in a wavelength range of 400−900 nm at room temperature. This system is illustrated in Figure 1a.

Acknowledgment. The authors thank Professor Eiichiro Ichishi and Associate Professor Yuzuru Takamura from Japan Advanced Institute of Science and Technology for valuable advice during the preparation of our manuscript.

Supporting Information Available: This material is available free of charge *via* the Internet at http://pubs.acs.org.

REFERENCES AND NOTES

1. Ghosh, S. K.; Kundu, S.; Mandal, M.; Pal, T. Silver and Gold Nanocluster Catalyzed Reduction of Methylene Blue by Arsine in a Micellar Medium. *Langmuir* **2002**, *18*, 8756–8760.
2. Kim, D.-K.; Kerman, K.; Saito, M.; Sathuluri, R. R.; Endo, T.; Yamamura, S.; Kwon, Y.-S.; Tamiya, E. Label-Free DNA Biosensor Based on Localized Surface Plasmon Resonance Coupled with Interferometry. *Anal. Chem.* **2007**, *79*, 1855–1864.
3. Ha, M. H.; Endo, T.; Saito, M.; Chikae, M.; Kim, D. K.; Yamamura, S.; Takamura, Y.; Tamiya, E. Label-Free Detection of Melittin Binding to a Membrane Using Electrochemical-Localized Surface Plasmon Resonance. *Anal. Chem.* **2008**, *80*, 1859–1864.
4. Endo, T.; Kerman, K.; Nagatani, N.; Takamura, Y.; Tamiya, E. Label-Free Detection of Peptide Nucleic Acid-DNA Hybridization Using Localized Surface Plasmon Resonance Based Optical Biosensor. *Anal. Chem.* **2005**, *77*, 6976–6986.
5. Wang, H.; Brandl, D. W.; Nordlander, P.; Halas, N. J. Plasmonic Nanostructures: Artificial Molecules. *Acc. Chem. Res.* **2007**, *40*, 53–62.
6. Hutter, E.; Fendler, J. H. Exploitation of Localized Surface Plasmon Resonance. *Adv. Mater.* **2004**, *16*, 1685–1706.
7. Willets, K. A.; Van Duyne, R. P. Localized Surface Plasmon Resonance Spectroscopy and Sensing. *Annu. Rev. Phys. Chem.* **2007**, *58*, 267–297.
8. Park, T. H.; Mirin, N.; Lassiter, J.; Hafner, J.; Halas, N. J.; Nordlander, P. Plasmonic properties of Nanoholes. *ACS Nano* **2008**, *2*, 25–32.
9. Anker, J. N.; Hall, W. P.; Lyandres, O.; Shah, N. C.; Zhao, J.; Van Duyne, R. P. Biosensing with plasmonic nanosensors. *Nat. Mater.* **2008**, *7*, 442–453.
10. Mayer, K. M.; Lee, S.; Liao, H.; Rostro, B. C.; Fuentes, A.; Scully, P. T.; Nehl, C. L.; Hafner, J. H. A Label-Free Immunoassay Based Upon Localized Surface Plasmon Resonance of Gold Nanorods. *ACS Nano* **2008**, *2*, 687–692.
11. Endo, T.; Kerman, K.; Nagatani, N.; Ha, M. H.; Kim, D. K.; Yonezawa, Y.; Nakano, K.; Tamiya, E. Multiple Label-Free Detection of Antigen-Antibody Reaction Using Localized Surface Plasmon Resonance-Based Core-Shell Structured Nanoparticle Layer Nanochip. *Anal. Chem.* **2006**, *78*, 6465–6475.

12. Ha, M. H.; Endo, T.; Kim, D. K.; Tamiya, E. Nanostructure and Molecular Interface for Biosensing Devices. *Proc. SPIE* **2007**, *6768*, 67680I1–67680I11.
13. Prasad, P. N. *Introduction to Biophotonics*; Wiley-Interscience: New York, 2003.
14. Gordon, R.; Sinton, D.; Kavanagh, K. L.; Brolo, A. G. A New Generation of Sensors Based on Extraordinary Optical Transmission. *Acc. Chem. Res.* **2008**, *41*, 1049–1057.
15. Haes, A. J.; Van Duyne, R. P. A Nanoscale Optical Biosensor: Sensitivity and Selectivity of an Approach Based on the Localized Surface Plasmon Resonance Spectroscopy of Triangular Silver Nanoparticles. *J. Am. Chem. Soc.* **2002**, *124*, 10596–10604.
16. Larsson, E. M.; Alegret, J.; Kall, M.; Sutherland, D. S. Sensing Characteristics of NIR Localized Surface Plasmon Resonances in Gold Nanorings for Application as Ultrasensitive Biosensors. *Nano Lett.* **2006**, *7*, 1256–1263.
17. Schwartz, M. P.; Alvarez, S. D.; Sailor, M. J. Porous SiO_2 Interferometric Biosensor for Quantitative Determination of Protein Interactions: Binding of Protein A to Immunoglobulins Derived from Different Species. *Anal. Chem.* **2007**, *79*, 327–334.
18. Lin, V. S. Y.; Motesharei, K.; Dancil, K. P. S.; Sailor, M. J.; Ghadiri, M. R. A Porous Silicon-Based Optical Interferometric Biosensor. *Science* **1997**, *278*, 840–843.
19. Nath, N.; Chilkoti, A. Label-Free Biosensing by Surface Plasmon Resonance of Nanoparticles on Glass: Optimization of Nanoparticle Size. *Anal. Chem.* **2004**, *76*, 5370–5378.
20. Fujiwara, K.; Watarai, H.; Itoh, H.; Nakahama, E.; Ogawa, N. Measurement of Antibody Binding to Protein Immobilized on Gold Nanoparticles by Localized Surface Plasmon Spectroscopy. *Anal. Bioanal. Chem.* **2006**, *386*, 639–644.
21. Macleod, H. A. *Thin-Film Optical Filters*; Macmillan: New York, 1986.
22. Palik, E. D. *Handbook of Optical Constants of Solids*; Academic Press: Orlando, FL, 1985.
23. Kreibig, U.; Vollmer, M. *Optical Properties of Metal Clusters*; Springer-Verlag: Berlin, 1995.
24. McMillan, B. G.; Berlouis, L. E. A.; Cruickshank, F. R.; Brevet, P. F. Reflectance and Electrolyte Electroreflectance from Gold Nanorod Arrays Embedded in a Porous Alumina Matrix. *J. Electroanal. Chem.* **2007**, *599*, 177–182.
25. Sheng, P. Theory for the Dielectric Function of Granular Composite Media. *Phys. Rev. Lett.* **1980**, *45*, 60–63.
26. Kalnin, J. R.; Kotomin, E. Modified Maxwell-Garnett Equation for the Effective Transport Coefficients in Inhomogeneous Media. *J. Phys. A: Math. Gen.* **1998**, *31*, 7227–7234.
27. Malinsky, M. D.; Kelly, K. L.; Schatz, G. C.; Van Duyne, R. P. Chain Length Dependence and Sensing Capabilities of the Localized Surface Plasmon Resonance of Silver Nanoparticles Chemically Modified with Alkanethiol Self-Assembled Monolayers. *J. Am. Chem. Soc.* **2001**, *123*, 1471–1482.
28. Lahav, M.; Vaskevich, A.; Rubinstein, I. Biological Sensing Using Transmission Surface Plasmon Resonance Spectroscopy. *Langmuir* **2004**, *20*, 7365–7367.
29. Huang, T. T.; Sturgis, J.; Gomez, R.; Geng, T.; Bashir, R.; Bhunia, A. K.; Robinson, J. P.; Ladisch, M. R. Composite Surface for Blocking Bacterial Adsoprtion on Protein Biochips. *Biotechnol. Bioeng.* **2003**, *81*, 618–624.
30. Peterfi, Z.; Kocsis, B. Comparison of Blocking Agents for an ELISA for LPS. *J. Immunoassay* **2000**, *21*, 341–354.
31. Paulsson, M.; Kober, M.; Freij-Larsson, C.; Sollenwerk, M.; Wesslen, B.; Ljungh, A. Adhesion of *Staphylococci* to Chemically Modified and Native Polymers, and the Influence of Preadsorbed Fibronectin, Vitronectin and Fibrinogen. *Biomaterials.* **1993**, *14*, 845–853.
32. Riboh, J. C.; Haes, A. J.; McFarland, A. D.; Yonzon, C. R.; Van Duyne, R. P. A Nanoscale Optical Biosensor: Real-Time Immunoassay in Physiological Buffer Enabled by Improved Nanoparticle Adhesion. *J. Phys. Chem. B* **2003**, *107*, 1772–1780.